Compaction of highly porous granular matter by impacts on a hard wall

Article *in* Physical Review E · April 2015

DOI: 10.1103/PhysRevE.91.042205

4 authors, including:

Nina Gunkelmann
Friedrich-Alexander-University of Erlangen-N…
20 PUBLICATIONS **70** CITATIONS
SEE PROFILE

E. M. Bringa
Universidad Nacional de Cuyo, Mendoza, Arg…
204 PUBLICATIONS **3,160** CITATIONS
SEE PROFILE

Compaction of highly porous granular matter by impacts on a hard wall

Christian Ringl,[1] Nina Gunkelmann,[1] Eduardo M. Bringa,[2] and Herbert M. Urbassek[1,*]

[1]*Physics Department and Research Center OPTIMAS, University Kaiserslautern, Erwin-Schrödinger-Straße, D-67663 Kaiserslautern, Germany*

[2]*CONICET and Facultad de Ciencias Exactas y Naturales, Universidad Nacional de Cuyo, Mendoza 5500, Argentina*

(Received 3 March 2015; published 30 April 2015)

Using a granular-mechanics code, we study the impact of a highly porous granular body on a hard wall. The projectile consists of monodisperse adhesive micrometer-sized silica grains. For the impact velocities studied, $v < 0.5$ m/s, the sample does not fragment, but is compacted. We find that the compaction is proportional to the impact speed. The proportionality constant increases with decreasing porosity. However, the compaction is inhomogeneous and decreases with distance from the target. A compaction wave runs through the aggregate; it slows down while the compaction becomes less efficient.

DOI: 10.1103/PhysRevE.91.042205 PACS number(s): 45.70.−n, 96.25.Pq, 95.30.Wi, 96.50.Dj

I. INTRODUCTION

Collisions of granular particles with hard walls are ubiquitous. They occur in the space environment, when interplanetary dust particles impact on the hard surfaces of moons, asteroids, or spacecraft [1,2]; they also happen in materials processing when granular matter interacts with the walls of the container [3–8]. Of special relevance is the particle-wall interaction in dedicated experiments which test the performance of granular aggregates by colliding them with a vibrating table, and use the results to deduce the aggregate properties [9–11].

Comminution milling, consisting of a single aggregate hitting a wall, is crucial in industrial applications (chemical, pharmaceutical, cement, food, mining, etc.). It is used to achieve grain size reduction and minimize the amount of fine and small fragments, since aggregate size determines its properties. Experiments to study this process are difficult, and mostly focus on the analysis of the fragment-size distribution after impact. The discrete element model method has been often used to study comminution [4,7,8,11].

Recently, dedicated collision experiments were performed with well-characterized aggregates with the aim of obtaining information on the properties of dust particles in space, and in particular on the evolution of the protoplanetary dust cloud. In such experiments Blum and coauthors studied the collision of individual silica grains or small agglomerates with velocities of around 1 m/s with flat surfaces [12,13]. In more recent experiments [14,15], the fragmentation distributions of granular clusters upon collision with a flat target were determined. In such experiments millimeter-sized dust aggregates are placed on a vibrating plate and thus perform multiple collisions with this plate. Since in multiple collisions, the cumulative compaction is larger than in a single collision it can more easily be measured [10].

Research on cluster-cluster collisions is somewhat more common than research on cluster-wall collisions. Experiments on grain-grain collisions include Refs. [5,16] and, in the astrophysical context, Ref. [17], where collision-induced compaction was measured. Collisions of relatively large (i.e., up to centimeter-sized) projectiles and targets were recently performed [18,19]. Experiments of centimeter-sized aggregates [20] showed that highly porous dust aggregates can retain their highly porous cores if collisions are highly energetic with collisions in the order of magnitude of 6 m/s and a dense shell forms on top of the porous core. Meisner *et al.* [21] studied agglomerate formation by impacts of submillimeter dust aggregates and found that the agglomerate density increases with speed and reaches values of up to 38% at 49 m/s impact speed.

Simulations on grain-grain collisions mainly measure collision-induced fragmentation [22] and only rarely analyze the compaction [23–25]. Recently a simulation study on the compaction induced by the impact of a hard sphere into a granular bed has been published [26].

Experimental and theoretical studies have recently been performed to investigate the formation of shock waves and the compaction in granular material. Bougie *et al.* [27] and Rericha *et al.* [28] studied the formation of shocks in a granular-gas flow colliding with a wedge and in oscillated granular layers, respectively. They accompany their studies with molecular-dynamics simulations. However, in contrast to our work, they concentrate on noncohesive matter, which allows them also to exploit similarities with Navier-Stokes-like continuum equations. This is justified in their work since they consider millimeter-sized grains. In our work, concentrating on micrometer-sized grains, friction and attractive intergranular forces are important and change the physical picture from a gaslike to a solidlike material. In particular, we do not have a steady compaction wave due to dissipative collisions. Cheng *et al.* [29] study granular jets hitting a target; also in their case, the simpler model of a noncohesive granular medium applies.

Our study will consider the aggregate-wall impact to occur in vacuum, such as it is relevant in the astrophysical context. We note, however, that interstitial gas contained in a granular aggregate will result in a strong drag force on particles during compaction due to the relative motion between the interstitial air and particles, and may hence influence the compression dynamics. Recent experiments have also demonstrated that interstitial gas contained in a granular target will affect the slowing-down forces [30,31]. A high gas content will induce the granular material to respond in a nearly incompressible,

*urbassek@rhrk.uni-kl.de; http://www.physik.uni-kl.de/urbassek/

fluidlike manner, while in the absence of gas the target is able to compact more strongly.

While previous work on collisions and compaction of granular matter concentrated on noncohesive matter, we study here adhesive matter. This is necessary since adhesive forces—and the friction accompanying them—are essential for understanding the properties and dynamics of granular matter composed of micrometer-sized grains, such as they are of interest here. The introduction of adhesive and friction forces considerably complicates the molecular-dynamics algorithm.

In the present paper, we apply our recently published model [32] for adhesive granular mechanics to the impact of a granular aggregate onto a hard wall of immobile particles. We choose the aggregate to be of a cuboidal form; since we use periodic boundary conditions in the lateral directions the projectile corresponds to a granular plane. A recent study [2] implemented a porosity model within a smoothed-particle hydrodynamics code, and the compaction wave traveling through a porous metallic cylinder was studied, with the aim of understanding collision and fragmentation of astrophysical bodies. In fact, understanding details of dust aggregate compaction could improve dust lifetime estimates in the interstellar medium [33]. Therefore, we focus on the compaction of the aggregate, its dependence on impact velocity, and on the homogeneity of the achieved compacted state.

II. METHOD

A. Granular-mechanics algorithm

We implemented our recent granular-mechanics algorithm [32] in the open-source code LIGGGHTS [34]. LIGGGHTS is an extension of the popular molecular-dynamics code LAMMPS [35] for the simulation of granular media. The acronym means "LAMMPS improved for general granular and granular heat transfer simulations." LIGGGHTS provides a high computational efficiency and is parallelized; it also offers advanced features, such as the use of complex geometries and the implementation of heat conduction between particles, which are not, however, used here.

Our code has been applied to simulate collisions of granular clusters [25], and the impact of a hard sphere into a granular bed [26]. The algorithm has been devised such as to be able to model systems containing large numbers ($>10^5$) of grains; therefore the collision dynamics contains simplifying assumptions, whose adequacy has been tested [25]. In the following we briefly describe the main features of our method.

Our clusters consist of spherical grains. All of them possess the same properties (radius R_{grain}, elastic moduli, etc.). The grains only interact if the distance of their centers $d < 2R_{\mathrm{grain}}$. As is common in granular mechanics, the length $\delta = 2R_{\mathrm{grain}} - d$ is called the grain *overlap*, and interactions are nonzero only for $\delta > 0$.

Forces between grains are classified as *normal* and *tangential forces*. The normal force consists of repulsive and adhesive contributions. The repulsive part [6],

$$f_{\mathrm{rep}} = \frac{4}{3} M \sqrt{R_{\mathrm{red}}\delta}(\delta + A v_n), \tag{1}$$

consists of a Hertzian $\delta^{3/2}$ contribution, based on elastic theory, and a dissipative part, describing a viscoelastic contact [36]. Here $R_{\mathrm{red}} = R_{\mathrm{grain}}/2$ is the reduced radius, $M = Y/2(1-\nu^2)$ is the reduced modulus, Y is Young's modulus, ν is Poisson's ratio, v_n is the velocity component in normal direction, and A is an empirical factor modeling dissipation. The adhesive part of the normal force is taken to be proportional to the specific surface energy [37–39],

$$f_{\mathrm{adh}} = 4\pi R_{\mathrm{red}} \gamma_{\mathrm{eff}}. \tag{2}$$

Here $\gamma_{\mathrm{eff}} = 2\gamma$ is the effective specific surface energy of the system, equal to twice the surface energy of a single grain.

Note that this value corresponds to the pull-off force of Derjaguin-Muller-Toporov (DMT) theory [37] needed to break a contact. We simplify the complex dependence of the adhesive force—as given by DMT [37] or Johnson-Kendall-Roberts (JKR) theory [40,41]—by a constant value [32]. In our approach, this value equals the pull-off force of DMT theory, which is valid for small particles with high elastic moduli (high rigidity), such as in our system. JKR theory is better suited to systems consisting of large grains with a low stiffness [38,42].

The tangential forces consist of several friction forces. Gliding friction,

$$f_{\mathrm{slide}} = \tfrac{1}{2} G \pi a^2, \tag{3}$$

depends on the shear modulus G and the radius $a = \sqrt{\delta R_{\mathrm{red}}}$ of the contact area [43]. Rolling motion is decelerated by a torque [44],

$$D_r = 2 f_{\mathrm{adh}} \xi_{\mathrm{yield}}. \tag{4}$$

Here, ξ_{yield} is the distance which two grains can roll over each other without breaking their atomic contacts. Finally, also torsional motion is decelerated by a torque, whose strength is given by [44]

$$D_t = \frac{1}{3} G \frac{a^3}{\pi}. \tag{5}$$

In the actual implementation, we supplement the velocity independent friction force, Eq. (3), with a velocity proportional contribution, valid for small velocities. This has the effect that the abrupt jump in the sliding force, which occurs when the tangential velocity approaches zero and leads to oscillations in the sign of the friction force from time step to time step, is smoothened. In detail, following [45] and [6], we write the tangential force f_t as

$$f_t = -\mathrm{sgn}(v_t)\min\{\eta_{\mathrm{tang}} v_t, f_{\mathrm{slide}}\}. \tag{6}$$

The value of the damping constant η_{tang} is chosen such that the above-mentioned oscillations do not occur. The choice of η_{tang} thus depends on the adopted time step, Δt, and is best determined by a test simulation. We found a value of $\eta_{\mathrm{tang}} = 0.1 m/\Delta t$ appropriate, where m is the grain mass. As a consequence, grain contact is stabilized. For the other friction forces we proceed analogously. For details see Ref. [32].

Our simulations have been performed with the well-documented molecular-dynamics package LIGGGHTS [34], with the addition of the above features.

B. System and simulation

We construct the projectiles as long cuboids with filling factors ranging from $\phi_0 = 13\%$ to $\phi_0 = 30\%$, which are typical values for some astrophysical applications [39]. The global filling factor of an ensemble of N grains—each with a volume $V_{\rm grain} = 4\pi R_{\rm grain}^3/3$—in a volume V is defined as $\langle\phi\rangle = N V_{\rm grain}/V$.

We build porous projectiles with a specified filling factor $\langle\phi\rangle_0$ as follows. First put a grain at an arbitrary position in the volume. Then

(1) calculate the local filling factor for each grain; this is done by counting the number of grains in a sphere of radius $5R_{\rm grain}$ around it;

(2) determine the grain with smallest local filling factor; if this choice is not unique, choose a grain at random among them;

(3) attach a grain to it in random direction; if the new grain overlaps with other grains, repeat this step;

(4) if the actual number of grains $< N$, go to step (1).

Step (3) is critical, and may lead to long computation times or even to the termination of the program. In practice, we avoid this by allowing only for a fixed number of attempts in step (3); then we jump back to step (2), choosing another grain with smallest local filling factor. For the highly porous aggregates used in this study, this step poses no problem. Note that the algorithm described here is only suitable for sufficiently large aggregates.

Grains may be kept inside the predefined volume by a number of methods. Most easily, in step (3) the insertion of a grain is not accepted, if it lies outside of the volume. Alternatively, a penalty may be introduced in this case—e.g., by an artificial increase of the local filling factor—which will prevent the aggregate from growing further at these grains.

A variant of this algorithm, which constructs fractal aggregates when the aggregate volume is not spatially confined, has recently been published [46]. We note that other methods to construct porous aggregates of given geometrical form start from regular (crystalline) clusters and have been summarized in Ref. [47].

Our cuboidal projectiles have a length of $250R_{\rm grain}$, and a width of $50R_{\rm grain}$; they contain $N = 20\,000$ to $N = 45\,000$ grains resulting in filling factors varying from $\langle\phi\rangle_0 = 0.13$ to $\langle\phi\rangle_0 = 0.3$.

The target is modeled as a plane consisting of immobile grains. The cuboid impacts with its axis perpendicular to the target (Fig. 1). We use periodic boundary conditions in the x and y directions to prevent lateral dilatation. With these boundary conditions we effectively consider the impact of a granular plane.

Our simulations last until the compaction wave has moved fully through the projectile. While the actual simulation time depends on the impact velocity, the minimum simulation time amounts to $10^7\Delta t = 0.5$ ms, where $\Delta t = 50$ ps is the simulation time step. In all cases we followed the dynamics until well after the compaction wave had passed through the entire projectile, such that we can be sure that no further changes in geometry and compaction can occur. As discussed elsewhere [32], the time step is short enough to ensure proper integration of the equations of motion.

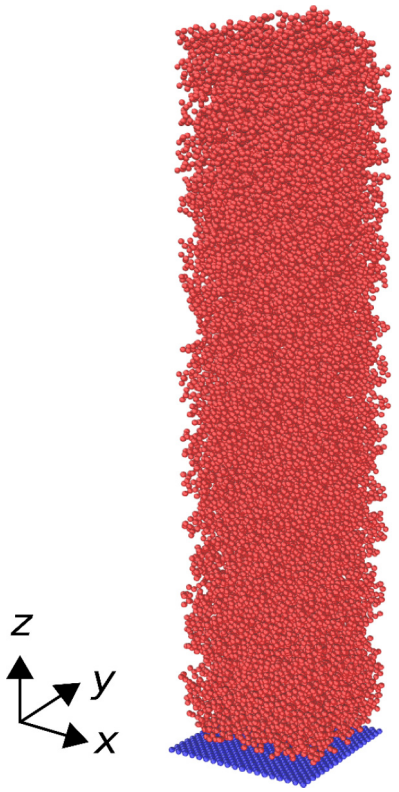

FIG. 1. (Color online) Snapshot of the initial configuration with filling factor $\langle\phi\rangle_0 = 0.2$. The granular projectile moves in the $-z$ direction towards the hard wall.

C. Parameter selection

Silica (SiO_2) is one of the main components of interstellar and interplanetary dust, and it is ubiquitous in several technological applications, for instance involving aerogel or glassy projectiles. Therefore, our grains are assumed to be made of silica, and the material parameters are chosen as appropriate for SiO_2 [48]: Young's modulus $Y = 54$ GPa, Poisson's ratio $\nu = 0.17$, shear modulus $G = Y/[2(1+\nu)]$, and $\gamma = 25$ mJ/m^2 is the surface energy of SiO_2.

The grain radius was kept fixed as $R_{\rm grain} = 0.76$ μm. This value was motivated by experimental work on the mechanical properties of porous granular aggregates in the astrophysical context [49]. The density of the SiO_2 grains amounts to $\rho = 2\times10^3$ kg m^{-3} [49]. The mass of a grain amounts to $m = 3.68\times10^{-15}$ kg. The dissipation constant A has been fitted to the experimentally measured [12] coefficient of restitution of silica grains; this gives $A = 0.5$ ns [32].

The value of the surface energy of silica assumed in the context of dust collisions in space varies in the region of 14–40 mJ/m^2 [48,50]. However, clean silica surfaces (in vacuum) have considerably higher surface energies of 300 mJ/m^2 [51]; the difference of more than a factor of 10 might be ascribed to the influence of surface contaminations, in particular adsorbed water [52,53]. In the context of protoplanetary clouds, it may often be safe to assume adsorbed layers; even in that situation, however, in close vicinity of stars (due to higher temperature and photodesorption), or after fresh fragmentation, surfaces may become clean. In the

context of molecular clouds, even the majority of silica grains may not be completely covered with adsorption layers. In the present work, we shall keep the surface energy at the value recommended in Ref. [48], $\gamma = 25\ \mathrm{mJ/m^2}$, in the lower range of possible values. We note, however, that the surface energy not only enters the adhesion force, but also rolling friction. In addition, due to the higher resulting equilibrium overlap, a higher dissipation in glide and torsional friction results. In Sec. III C, we shall explore the influence of a change of γ on the compaction process. We also note that changes in adhesion can cause changes in the size distributions of a collection of colliding grains [54].

III. RESULTS

A. Compaction

The collision velocities studied by us ($v \leqslant 0.35$ m/s) are chosen so small that the granular body does not fragment. Figure 2 demonstrates that the length Z of the sample strongly decreases after impact, and the decrease grows monotonically

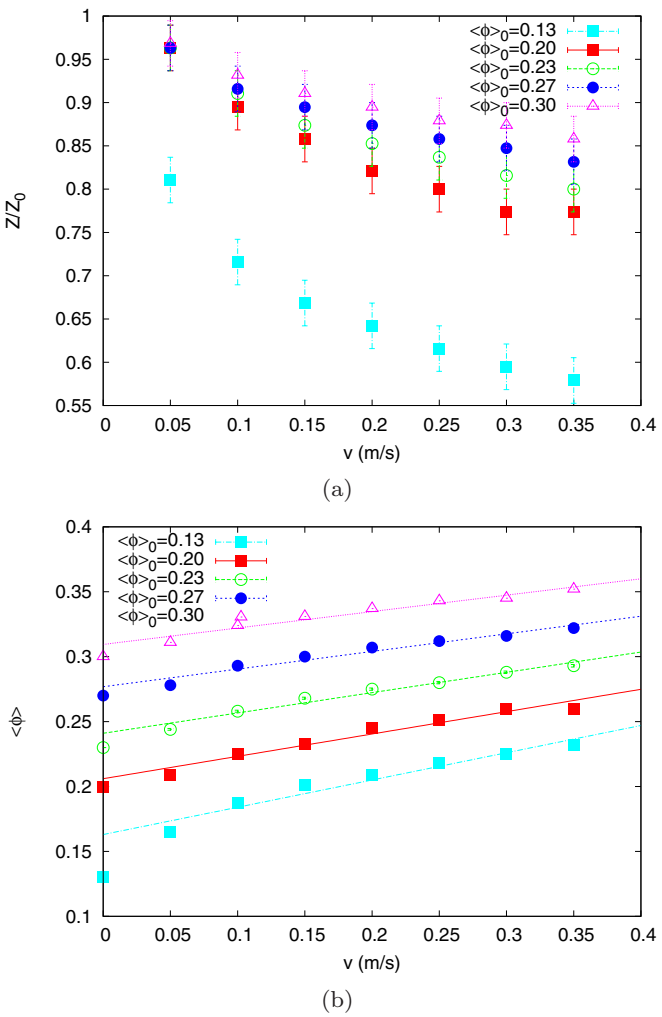

FIG. 2. (Color online) (a) Change in relative length Z/Z_0 and (b) global filling factor $\langle\phi\rangle$ of the aggregate after impact with velocity v for various initial porosities. The fit lines in (b) are linear laws, Eq. (7).

TABLE I. Parameters $\langle\bar{\phi}\rangle_0$ and α describing the velocity dependence of compaction, Eq. (7). The error in $\langle\bar{\phi}\rangle_0$ is below 0.005, and in α below 0.02 s/m.

$\langle\phi\rangle_0$	0.13	0.20	0.23	0.27	0.30
$\langle\bar{\phi}\rangle_0$	0.16	0.21	0.24	0.28	0.31
α (s/m)	0.21	0.17	0.16	0.14	0.13

with impact speed. The particularly strong initial decrease for the thinnest aggregate is due to its "fluffy" surface which strongly compacts when contacting the wall. We determine Z as the value where the density has decreased to $1/e$ of the bulk density; here the local density, $\phi(z)$, has been determined by cutting the body in slices of $5.3R_{\mathrm{grain}}$ thickness.

The changed dimensions can be used to calculate the filling factor of the aggregate after the collision for different initial porosities. Our results, Fig. 2(b), demonstrate that the global filling factor $\langle\phi\rangle$ increases roughly linearly with impact velocity v,

$$\langle\phi\rangle = \langle\bar{\phi}\rangle_0 + \alpha v. \tag{7}$$

The linear increase with velocity is in line with recent experiments performed on agglomerate formation by impacts of submillimeter dust aggregates [21]; these authors find a linear increase of the average filling factor of the aggregate at impact velocities below 10 m/s.

The fit factors α and $\langle\bar{\phi}\rangle_0$ are assembled in Table I. Note that $\langle\bar{\phi}\rangle_0$ is very close to the initial filling factor of the sample, $\langle\phi\rangle_0$, as it should be; nevertheless, we kept it as a fit factor in order to improve the quality of the fit. The constant α increases with decreasing $\langle\phi\rangle_0$, as expected.

This result qualitatively agrees with collision experiments of dust aggregates [20] where the filling factor was found to increase with impact velocity. A quantitative comparison is not possible because our aggregates are significantly smaller. For our smaller samples, we observe higher compaction because the aggregates possess more energy and can restructure more efficiently.

Figure 3 shows the depth dependence of the compaction. For small velocities, the compaction is quite homogeneous throughout the sample length. Upon closer inspection, the density profile in the aggregate tends to decrease somewhat away from the impact point. This trend becomes more pronounced for higher velocities. In good approximation, the filling factor inside the collided sample decreases linearly with the distance from the impact point, z,

$$\phi(z) = \phi(0) - az/R_{\mathrm{grain}}. \tag{8}$$

The dependence of the parameters is plotted in Fig. 4. It shows that the inhomogeneity of compaction increases with velocity so that both a and $\phi(0)$ increase with increasing velocity. The effect is stronger for lower initial porosities. The reason for the inhomogeneous density profile lies in the attenuation of the compaction wave which will be described in the next section.

The increase of the maximum filling factor, $\phi(0)$, with velocity follows well a linear law; only for the smallest velocities—and here in particular for the thinnest aggregate—we see deviations from linearity. These linear laws are included

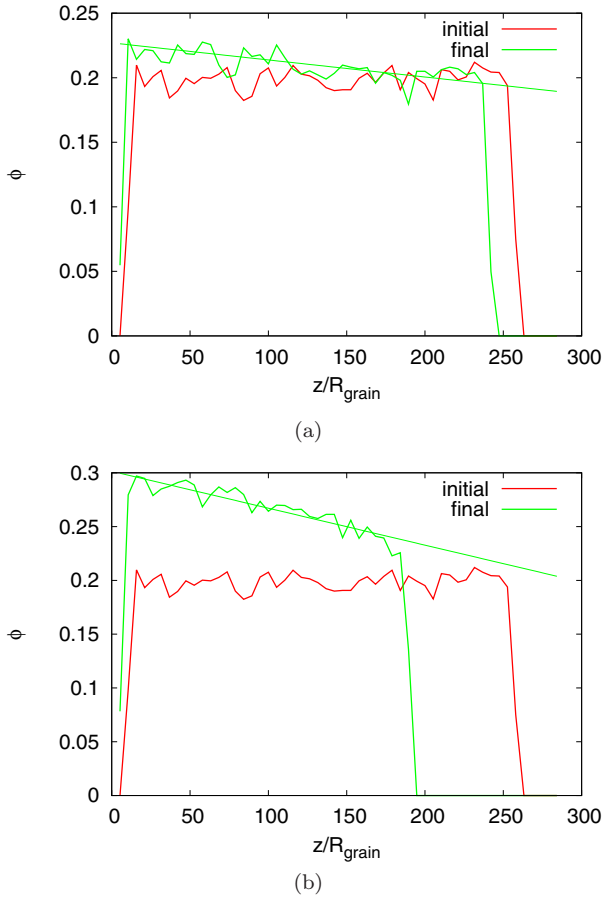

FIG. 3. (Color online) Local filling factor of the aggregate, $\phi(z)$, as a function of distance z from the wall before ("initial") and after ("final") the collision. Impact velocity is (a) $v = 0.05$ and (b) $v = 0.35$ m/s. The initial filling factor was $\langle\phi\rangle_0 = 0.2$. Lines show a linear trend, Eq. (8).

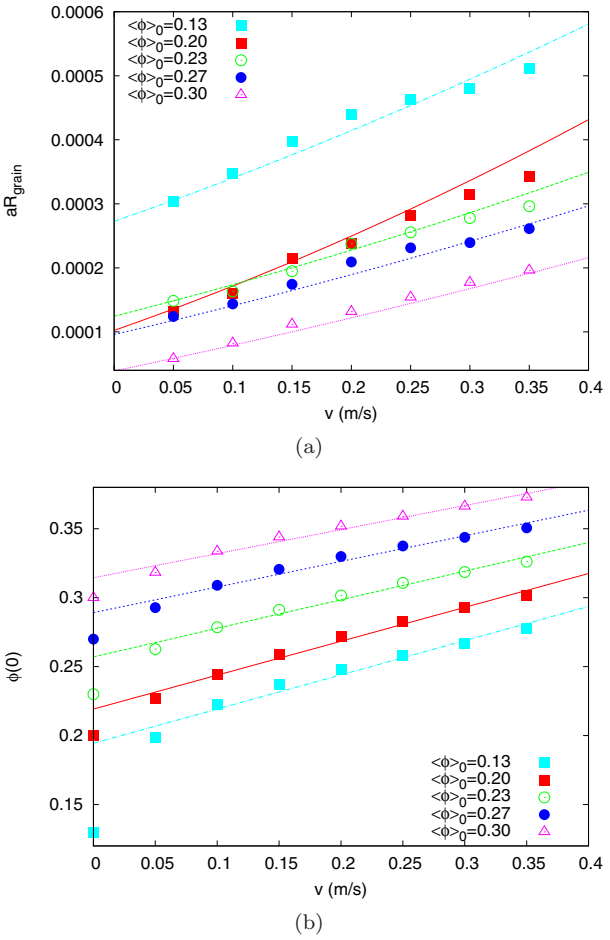

FIG. 4. (Color online) Dependence of the parameters (a) a and (b) $\phi(0)$, which describe the inhomogeneity of compaction, Eq. (8), on the impact velocity v for various initial porosities, $\langle\phi\rangle_0$. The lines in (b) are linear fits; the lines in (a) are calculated from these fits by making use of mass conservation, Eq. (7).

in Fig. 4(b). By virtue of Eq. (7), which describes the velocity dependence of the average filling factor, the coefficient a is not independent of ϕ_0 but can be evaluated from it; the resulting prediction is included in Fig. 4(a). This argument explains how the linear velocity dependence in Eq. (7) translates to (approximately) linear dependencies also for the coefficients describing the inhomogeneous density profiles in the collided aggregates, Eq. (8).

B. Compaction wave

While the projectile is colliding with the wall, a compaction wave runs through the aggregate. Figure 5 shows a detailed view of the cuboid during the collision and highlights the velocity of the compaction wave. At 100 μs after the impact the upper part of the cuboid still moves with its impact velocity $v = 0.2$ m/s towards the wall, while the lower part has already been stopped. Concomitantly with the deceleration, grains have been compacted. In the bottom part we see a clear velocity gradient. At 300 μs the aggregate has been stopped in its entire length.

Figure 6(a) shows a typical spatial profile of the particle velocity in the z direction. No steady shock front is formed but the velocity of the particles smoothly decreases with

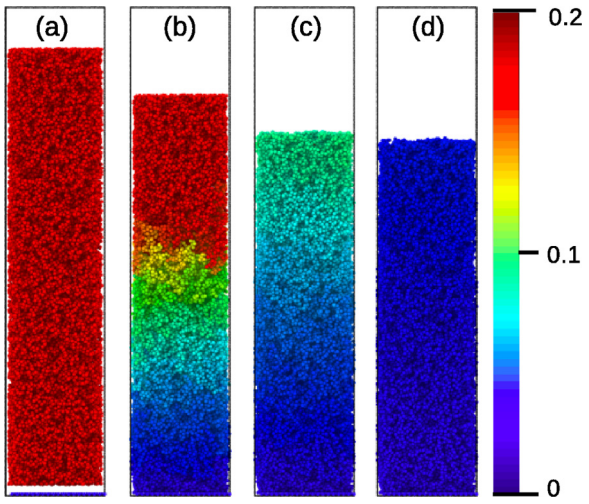

FIG. 5. (Color online) Snapshots of the projectile (a) immediately before impact, and at (b) 100, (c) 200, and (d) 300 μs after impact. The aggregate has an initial velocity of $v = 0.2$ m/s and a filling factor of $\langle\phi\rangle_0 = 0.2$. Color codes the grain velocity v_z in m/s.

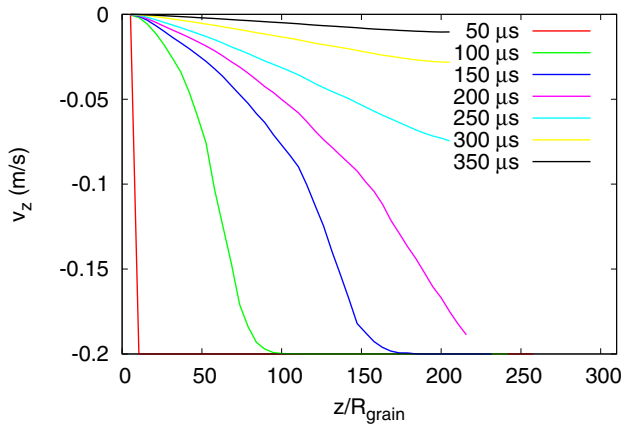

(a)

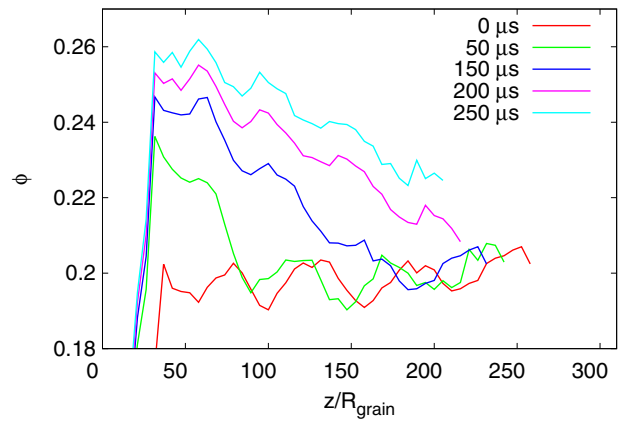

(b)

FIG. 6. (Color online) Spatial profiles for an aggregate with initial filling factor $\langle\phi\rangle_0 = 0.2$ and initial velocity $v = 0.2$ m/s showing (a) the grain velocity in the z direction and (b) the local filling factor. Curves in (b) are smoothed by moving averages which replace each data value with the average of four neighboring values.

distance from the target, z, coincident with the inhomogeneity of the filling factor (see Fig. 4). Figure 6(b) shows the spatial profile of the local filling factor for various simulation times. The evolution of the inhomogeneous density profile becomes clearly visible in this figure, Fig. 6(b). The local filling factor at the wall itself, $\phi(0)$, increases with time until its final value is reached. As an example for a transient state consider the compaction at time 50 μs after impact; the front part of the projectile is already compressed, while at depths $> 100R_{\text{grain}}$, the projectile still has retained its original density.

We can evaluate the velocity of the compaction wave, V, by determining the time dependence of the wave front visible in Fig. 5. In detail we consider the time dependence of the position where the particle velocity deviates (by at least 1%) from the impact velocity; we consider this to be the wave front. The data are plotted in Fig. 7. The compacting wave velocities are around 1 m/s, considerably larger than the impact velocity itself. We note that this velocity is substantially smaller than estimated sound velocities in granular aggregates similar to ours [32]; this work gives a value of around 50 m/s. We note that we were not able to determine the speed of sound for

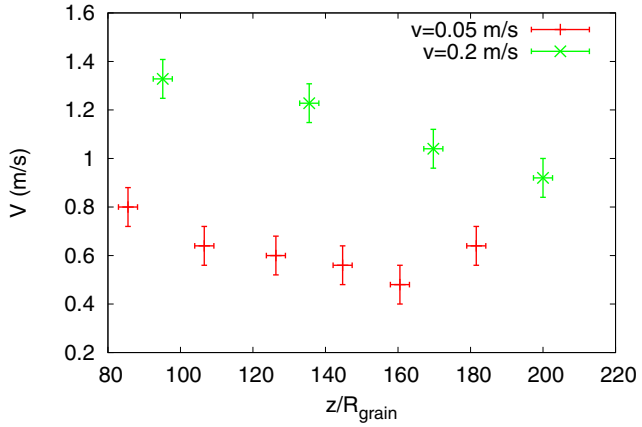

FIG. 7. (Color online) Compaction wave velocity in dependence of the distance z from the target with impact velocities $v = 0.05$ m/s and $v = 0.2$ m/s and filling factor $\langle\phi\rangle_0 = 0.2$.

our aggregates in our simulations, due to the strong energy dissipation present.

The theoretical evaluation of the speed of the compaction wave is not straightforward because in our case it is nonstationary. Analytical and simulation studies usually consider steady compaction waves in porous materials (see, for instance, [55,56]). Such models admit both subsonic and supersonic steady compaction waves but for subsonic waves no leading shock is predicted.

Figure 7 also shows that the compaction wave velocity decreases with distance from the wall; this is caused by the energy dissipation occurring in the sample. We also observe that the compaction wave speed V increases with increasing impact velocity v.

C. Influence of surface energy

The size of the surface energy, γ, will influence the compaction process. In order to investigate this influence, we performed simulations in which γ was varied between 5 and 45 mJ/m^2 around the nominal value of 25 mJ/m^2, for which this model was set up. In this study, the granular projectile always impacts with a velocity of 0.15 m/s.

We note that according to Sec. II A, γ influences the dynamics in two respects since (i) the adhesion force, Eq. (2), and (ii) the rolling friction, Eq. (4), are proportional to γ.

We observe in Fig. 8 that the impact-induced compaction decreases monotonically with γ. In fact, with the exception of the smaller values of γ, our data can be well fitted by a linear dependence in the range of values investigated. We explain this dependence qualitatively with the decreasing rolling friction, which grains experience; thus a smaller value of γ allows them to change contacts more easily and hence to compact more. When increasing the surface energy above the largest value shown in Fig. 8—we simulated values up to 1000 mJ/m^2—the compaction stays the same as for the largest value shown in Fig. 8, $\gamma = 45$ mJ/m^2. Here, we are in the regime where friction is governed by the viscous component of Eq. (6); hence an initial amount of compaction occurs even for highly adhesive grains. With these simulations we are already beyond the limit of validity of our numerical model.

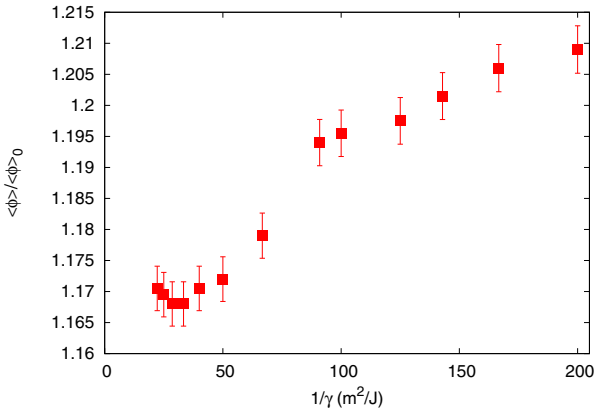

FIG. 8. (Color online) Influence of the surface energy of grains, γ, on the compaction. Data are for an impact velocity of $v = 0.15$ m/s and an initial filling factor of $\langle\phi\rangle_0 = 0.2$.

In the limit of vanishing γ, the projectile is no longer adhesive and falls apart when touching the wall. In our simulation this happens when $\gamma \lesssim 0.6$ mJ/m^2. This means, in particular, that within our model we cannot study the transition to noncohesive materials. Note that in other work on compaction of noncohesive granular material, gravity is included which forces the material to the surface, while a boundary vessel (or a laterally infinitely extended layer) prohibits the material to flow apart sideways [57,58].

IV. CONCLUSIONS

Using a granular-mechanics code, we study the impact of a granular body consisting of adhesive monodisperse micrometer-sized silica grains on a hard wall. The model includes elastic repulsive, adhesive, and dissipative forces, as well as sliding, rolling, and twisting friction. Impact velocities $v < 0.5$ m/s are studied, for which the aggregate does not fragment. Projectile filling factors between 13% and 30% are studied. We find

(1) The granular aggregate is compacted. Compaction is proportional to the impact speed. The constant of proportionality increases with decreasing porosity.

(2) With increasing impact velocity v, compaction starts decreasing linearly away from the target. The effect increases with increasing velocity and is stronger for lower initial porosities.

(3) A compaction wave runs through the aggregate with decreasing velocity. The wave velocity is considerably smaller than the speed of sound.

(4) The reason for the inhomogeneous density profile lies in the attenuation of the compaction wave.

Collisions of granular material with hard walls are important for industrial [11,59] and astrophysical applications [2,10,12–15,33], which typically focus on fragmentation. However, compaction is an important factor, changing mechanical properties and also steady state size distributions [4]. This is the reason why we focus on compaction in this study, and our findings on compaction saturation might help design better comminution methods and establish constraints on astrophysical studies of grain evolution.

ACKNOWLEDGMENTS

This work has been supported by the Deutsche Forschungsgemeinschaft via the Graduiertenkolleg 814. E.M.B. acknowledges support from CONICET, SeCTyP (U.N. Cuyo), and PICT-PRH 0092 from ANPCyT (Agencia Nacional de Promocion Cientifica y Tecnologica, Argentina). Simulations were performed at the High Performance Cluster Elwetritsch (RHRK, TU Kaiserslautern, Germany).

[1] E. Grün, in *Encyclopedia of the Solar System*, 2nd ed., edited by L. A. McFadden, P. R. Weissman, and T. V. Johnson (Academic, New York, 2007), p. 621.
[2] M. Jutzi, W. Benz, and P. Michel, Icarus **198**, 242 (2008).
[3] J. Duran, *Sands, Powders, and Grains: An Introduction to the Physics of Granular Materials* (Springer-Verlag, Berlin, 2000).
[4] B. K. Mishra and C. Thornton, Int. J. Miner. Process. **61**, 225 (2001).
[5] G. K. Reynolds, J. S. Fu, Y. S. Cheong, M. J. Hounslow, and A. D. Salman, Chem. Eng. Sci. **60**, 3969 (2005).
[6] T. Pöschel and T. Schwager, *Computational Granular Dynamics: Models and Algorithms* (Springer, New York, 2005).
[7] H. A. Carmona, F. K. Wittel, F. Kun, and H. J. Herrmann, Phys. Rev. E **77**, 051302 (2008).
[8] Z. B. Tong, R. Y. Yang, A. B. Yu, S. Adi, and H. K. Chan, Powder Technol. **196**, 213 (2009).
[9] K. Hein, T. Hucke, M. Stintz, and S. Ripperger, Part. Part. Syst. Charact. **19**, 269 (2002).
[10] R. Weidling, C. Güttler, J. Blum, and F. Brauer, Astrophys. J. **696**, 2036 (2009).
[11] F. K. Wittel, Granular Matter **12**, 447 (2010).
[12] T. Poppe, J. Blum, and T. Henning, Astrophys. J. **533**, 454 (2000).
[13] J. Blum and G. Wurm, Icarus **143**, 138 (2000).
[14] C. Güttler, J. Blum, A. Zsom, C. W. Ormel, and C. P. Dullemond, Astron. Astrophys. **513**, A56 (2010).
[15] R. J. Geretshauser, R. Speith, C. Güttler, M. Krause, and J. Blum, Astron. Astrophys. **513**, A58 (2010).
[16] J. Subero and M. Ghadiri, Powder Technol. **120**, 232 (2001).
[17] J. Teiser and G. Wurm, Mon. Not. R. Astron. Soc. **393**, 1584 (2009).
[18] D. Langkowski, J. Teiser, and J. Blum, Astrophys. J. **675**, 764 (2008).
[19] E. Beitz, C. Güttler, J. Blum, T. Meisner, J. Teiser, and G. Wurm, Astrophys. J. **736**, 34 (2011).
[20] T. Meisner, G. Wurm, and J. Teiser, Astron. Astrophys. **544**, A138 (2012).
[21] T. Meisner, G. Wurm, J. Teiser, and M. Schywek, Astron. Astrophys. **559**, A123 (2013).
[22] L. Liu, K. D. Kafui, and C. Thornton, Powder Technol. **199**, 189 (2010).

[23] D. Paszun and C. Dominik, Astron. Astrophys. **507**, 1023 (2009).
[24] K. Wada, H. Tanaka, T. Suyama, H. Kimura, and T. Yamamoto, Astrophys. J. **677**, 1296 (2008).
[25] C. Ringl, E. M. Bringa, D. S. Bertoldi, and H. M. Urbassek, Astrophys. J. **752**, 151 (2012).
[26] C. Ringl, E. M. Bringa, and H. M. Urbassek, Phys. Rev. E **86**, 061313 (2012).
[27] J. Bougie, Sung Joon Moon, J. B. Swift, and H. L. Swinney, Phys. Rev. E **66**, 051301 (2002).
[28] E. C. Rericha, C. Bizon, M. D. Shattuck, and H. L. Swinney, Phys. Rev. Lett. **88**, 014302 (2001).
[29] X. Cheng, G. Varas, D. Citron, H. M. Jaeger, and S. R. Nagel, Phys. Rev. Lett. **99**, 188001 (2007).
[30] J. R. Royer, E. I. Corwin, P. J. Eng, and H. M. Jaeger, Phys. Rev. Lett. **99**, 038003 (2007).
[31] G. Caballero, R. Bergmann, D. van der Meer, A. Prosperetti, and D. Lohse, Phys. Rev. Lett. **99**, 018001 (2007).
[32] C. Ringl and H. M. Urbassek, Comput. Phys. Commun. **183**, 986 (2012).
[33] A. P. Jones and J. A. Nuth, Astron. Astrophys. **530**, A44 (2011).
[34] C. Kloss, C. Goniva, A. Hager, S. Amberger, and S. Pirker, Prog. Comput. Fluid Dyn. **12**, 140 (2012).
[35] S. Plimpton, J. Comput. Phys. **117**, 1 (1995). http://lammps.sandia.gov/.
[36] N. V. Brilliantov, F. Spahn, J.-M. Hertzsch, and T. Pöschel, Phys. Rev. E **53**, 5382 (1996).
[37] B. V. Derjaguin, V. M. Muller, and Y. P. Toporov, J. Colloid Interface Sci. **53**, 314 (1975).
[38] D. Maugis, *Contact, Adhesion and Rupture of Elastic Solids* (Springer, Berlin, 2000).
[39] J. Blum, Adv. Phys. **55**, 881 (2006).
[40] K. L. Johnson, K. Kendall, and A. D. Roberts, Proc. R. Soc. London, Ser. A **324**, 301 (1971).
[41] K. L. Johnson, *Contact Mechanics* (Cambridge University Press, Cambridge, 1985).
[42] D. Maugis, J. Colloid Interface Sci. **150**, 243 (1992).
[43] N. Burnham and A. A. Kulik, in *Handbook of Micro/Nano Tribology*, 2nd ed., edited by B. Bhushan (CRC Press, Boca Raton, 1999), Chap. 5, p. 247.
[44] C. Dominik and A. G. G. M. Tielens, Astrophys. J. **480**, 647 (1997).
[45] P. K. Haff and B. T. Werner, Powder Technol. **48**, 239 (1986).
[46] C. Ringl and H. M. Urbassek, Comput. Phys. Commun. **184**, 1683 (2013).
[47] K. Wada, H. Tanaka, T. Suyama, H. Kimura, and T. Yamamoto, Astrophys. J. **737**, 36 (2011).
[48] A. Chokshi, A. G. G. M. Tielens, and D. Hollenbach, Astrophys. J. **407**, 806 (1993).
[49] J. Blum and R. Schräpler, Phys. Rev. Lett. **93**, 115503 (2004).
[50] L.-O. Heim, J. Blum, M. Preuss, and H.-J. Butt, Phys. Rev. Lett. **83**, 3328 (1999).
[51] J. Mizele, J. L. Dandurand, and J. Schott, Surf. Sci. **162**, 830 (1985).
[52] K. Kendall, N. M. Alford, and J. D. Birchall, Nature (London) **325**, 794 (1987).
[53] K. Kendall, N. M. Alford, and J. D. Birchall, Proc. R. Soc. London, Ser. A **412**, 269 (1987).
[54] A. H. F. Guimarães, N. Albers, F. Spahn, M. Seiß, E. Vieira-Neto, and N. V. Brilliantov, Icarus **220**, 660 (2012).
[55] J. M. Powers, D. S. Stewart, and H. Krier, Trans. ASME **56**, 15 (1989).
[56] R. Menikoff, in *23rd International Symposium on Shock waves, 2001*, paper 5016, Technical Report No. LA-UR-01-2211, Los Alamos National Laboratory, 2001.
[57] P. Philippe and D. Bideau, Phys. Rev. Lett. **91**, 104302 (2003).
[58] P. Ribière, P. Richard, R. Delannay, and D. Bideau, Phys. Rev. E **71**, 011304 (2005).
[59] H. P. Zhu, Z. Y. Zhou, R. Y. Yang, and A. B. Yu, Chem. Eng. Sci. **63**, 5728 (2008).